Deep hydrodesulfurization of 4,6-dimethydibenzothiophene over CoMoS/ TiO2 catalysts: Impact of the TiO2 treatment

Teddy Roy, Julie Rousseau, Antoine Daudin, Gerhard Pirngruber, Benedicte Lebeau, Jean-Luc Blin, Sylvette Brunet

Deep hydrodesulfurization of 4,6-dimethydibenzothiophene over CoMoS/TiO_2 catalysts: Impact of the TiO_2 treatment

Teddy Roy[a], Julie Rousseau[a], Antoine Daudin[b], Gerhard Pirngruber[b], Benedicte Lebeau[c], Jean-Luc Blin[d*], Sylvette Brunet[a*]:

[a] : Université de Poitiers /CNRS, IC2MP, UMR 7285, 86073 Poitiers Cedex 9 France.

[b] : IFP Energies nouvelles, Rond-point de l'échangeur de Solaize, BP 3, 69360 Solaize, France

[c]: Université de Haute Alsace (UHA)/CNRS, IS2M, UMR 7361, 68093 Mulhouse cedex, France

[d] : Université de Lorraine/CNRS, L2CM, UMR7053, F-54506 Vandoeuvre-lès-Nancy cedex, France

Corresponding authors

Dr. Sylvette Brunet
Institut de Chimie des Milieux et Matériaux de Poitiers (IC2MP) CNRS 7285
Université de Poitiers
B27-4 rue Michel Brunet TSA 51106 86073 Poitiers Cedex 9 France
tel: +33 5 49 45 36 27
E-mail: sylvette.brunet@univ-poitiers.fr

Pr. Jean-Luc Blin
Université de Lorraine
L2CM UMR CNRS 7053
Faculté des Sciences et Technologies
BP 70239
F-54506 Vandoeuvre-lès-Nancy cedex, France
Tel. +33 3 83 68 43 70
E-mail: Jean-Luc.Blin@univ-lorraine.fr

Graphical Abstract

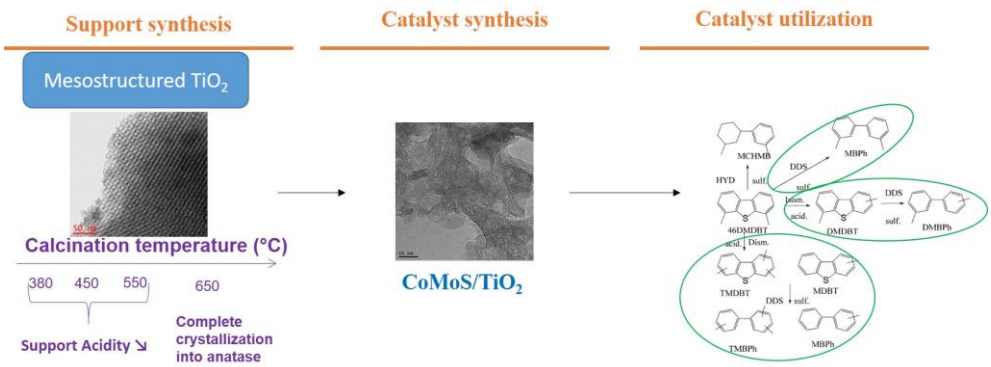

Abstract

Mesostructured titania as support for the CoMoS active phase in deep hydrodesulfurization (HDS) of 4,6-dimethydibenzothiophene (4,6-DMDBT) leads to an increase of the intrinsic HDS activity and a higher selectivity for direct desulfurization (DDS) for HDS reaction in contrast with the conventional CoMoS/alumina catalyst. The temperature treatment of the mesostructured TiO_2 support, modifies the catalyst's activity for the transformation of 4,6-DMDBT. The higher total and HDS activities were obtained after treatment at 380°C corresponding to the higher specific surface area and to a mesostructured TiO_2 material with a semi-crystalline anatase framework. Beyond 550°C, the specific surface area decreases strongly corresponding to a complete crystallization of the mesopores walls into anatase structure. Moreover, the temperature under which the support is treated prior its impregnation has no impact on the selectivity of the transformation routes of the sulfur compound.

Keywords: Mesoporous titania, Brønsted acidity, Hydrodesulfurization, Dismutation, Isomerization, 4,6-Dimethyldibenzothiophene

1. Introduction

One of the major issue of our society is the reduced quality of air due to atmospheric pollution, mainly in urbans area. Emissions from transports are one of the most important factors contributing to the atmospheric pollution due to nitrogen oxides (NO_x) and sulfur oxides (SO_x). In order to deal with this issue, stringent regulations have been set up and are challenging researchers to develop highly active and stable catalysts to produce cleaner fuels. Indeed, since 2009, the regulation imposed sulfur level in gas oils lower than 10 ppm [1]. To cope with this legislation, refiners have developed the deep hydrodesulfurization (HDS) for removing sulfur-containing compounds to obtain ultra-low sulfur fuels. It is well established that the sulfur compounds present in diesel fuels at sulfur levels of less than 250 ppm are mainly dibenzothiophenes and alkyldibenzothiophenes, with 4,6-dimethydibenzothiophene (4,6-DMDBT) usually used as model molecule for HDS refractory compounds [2-8]. The transformation pathways of the latter are also well established (Scheme 1). Three routes have been reported in the literature: the hydrogenation (HYD) route, hydrogenating a benzene ring before the cleavage of C-S bond, the direct desulfurization (DDS) route, directly cleaving the C-S bond and the acidic route (DDS Acid) including isomerization and/or dismutation reactions of the methyl groups. The latter route is only observed on supported catalysts containing Brønsted acidity, particularly zeolites alone or in mixture [9-10]. HDS is commonly performed at medium temperature (340 °C) and under hydrogen pressure (3-4 MPa) over a heterogeneous catalyst, usually CoMo over alumina. The active phase of the catalyst consists of supported MoS_2 slabs on γ-alumina promoted by cobalt. Over a conventional catalyst $CoMo/Al_2O_3$, the main transformation pathway of 4,6-DMDBT is following the HYD route. Much researches have been reported in order to optimize this process, one option is to design different supports. Indeed, the experts in the field are aware of the fact that the surface chemistry of alumina is not really optimal for the preparation of

highly active promoted MoS_2 catalysts. The strong interaction of transition metals such as Mo, Ni or Co with the alumina support impedes full sulfidation and hence limits activity [11]. Other supports like silica, zeolites, carbon, titania, and mixed metal oxides are reported to provide significant improvements compared to γ-Al_2O_3 [12-17]. Among all these supports, TiO_2 is particularly intriguing [18-21]. For example, Klimova et al. [20] have shown that NiMo catalysts supported on titania nanotubes allowed reaching high conversions of 4,6-DMDBT with a much lower proportion of hydrogenated product than using NiMo/γAl_2O_3 catalyst. Castillo et al. [21], have also reported that the addition of TiO_2 to the surface of alumina involves the dispersion of the well-sulfided active phase and hence in catalytic activity. However, it is rarely used as a support mainly because of its low specific surface area (50 $m^2\ g^{-1}$ against 230 $m^2\ g^{-1}$ for γ-Al_2O_3), thermal stability and mechanical strength. A simple method, combining the sol-gel process and the surfactant templating method, to prepare mesostructured titania with high specific area (> 250 $m^2\ g^{-1}$) has been reported [~~20-23~~ 22-25]. In a recent paper, we have shown that a higher DDS selectivity for the HDS of 4,6-DMDBT was observed with CoMoS supported over mesostructured TiO_2 [19]. This shift towards DDS selectivity in the transformation of 4,6-DMDBT is unprecedented in literature. Moreover, it involves Brønsted acidity of the support, which likely influences the nature of the formed intermediates. In addition, isomerization and dismutation reactions, which are catalyzed by Brønsted acid sites also participate to the shift towards DDS selectivity as observed on a zeolite support [9].

This paper deals with the identification of the parameters involved in the change of selectivity of the various pathways (HYD and DDS) in the HDS of the sulfur model compound (4,6-DMDBT) over CoMoS supported over mesostructured titania catalysts. In this way, the effect of the thermal treatment of the support prior the deposition of the active phase has been studied. The results are compared with the ones obtained using the conventional

$CoMoS/Al_2O_3$ catalyst and the CoMoS/P25 one, used as a reference titania support. In order to explain the catalytic results, characterizations of the active phase and Brønsted acidity were investigated.

2. Materials and methods

Cobalt(II) nitrate hexahydrate ($CoN_2O_6.6H_2O$, 99.00 % Sigma-Aldrich) and ammonium heptamolybdate [$(NH_4)_6Mo_7.6H_2O$, 99.98 % Sigma-Aldrich] were used as Co and Mo precursors, respectively.

2.1. Supports and catalyst preparation.

Mesostructured titania have been synthesized according to the procedure reported in previous work using the triblock copolymer P123 $(EO)_{20}(PO)_{70}(EO)_{20}$ (labeled as P123) as surfactant [18-19]. To investigate the effect of thermal treatment temperature on the support properties and thus on the catalyst performance, the final mesostructured TiO_2 support (after Soxhlet extraction using ethanol) is treated at different temperatures from 380°C to 650°C for 1h under synthetic air atmosphere.

Supported CoMo catalysts over as-synthesized mesostructured titania and commercial P25 (powders) were prepared by incipient wetness impregnation using cobalt(II) nitrate hexahydrate ($Co(NO_3)_2.6H_2O$, 99.00 % Sigma-Aldrich) and ammonium heptamolybdate [$(NH_4)_6Mo_7.4H_2O$, 99.98 % Sigma-Aldrich] precursors in aqueous solution. The targeted number of Mo atoms per nm^2 and the Co/Mo ratio were fixed to 3 and 0.54, respectively. The precursors were then decomposed at 380°C under air during 5 hours.

2.2. Catalytic measurements:

Dimethyl disulfide (>99% purity), 4,6-DMDBT (>95% purity) and n-heptane (>99% purity) from Aldrich Chemicals were used without further purification.

As reported in previous papers [18,19], the catalysts are sulfided *in situ* in a fixed flow reactor using a sulfiding feed made of 5 % wt of dimethyl disulfide (DMDS) in n-heptane as solvent at a temperature of 350°C under a 4.0 MPa of total pressure during 14 hours. The temperature was then lowered to the reaction temperature (340°C).

Then, HDS of 4,6-DMDBT was carried out at 340°C and 4.0 MPa of total pressure after the *in situ* sulfidation of the catalyst according to the procedure described above. The feed was composed by 4,6-DMDBT (500 ppm S) diluted in n-heptane into which dimethyl disulfide (9500 ppm S) was added to generate H_2S.

Different activities (A) were considered. They are defined as the number of moles of sulfur compounds transformed by each route for the transformation of 4,6-DMDBT per gram of catalyst, per m² and per molybdenum atom. A_{Total} corresponds to the total activity, the sum of acid activity and hydrodesulfurization activity. The different activities are defined as follow: A_{acid} represents the activity for isomerization and dismutation of 4,6-DMDBT into alkyldibenzothiophenes. A_{HDS} is related to the total activity for 4,6-DMDBT corresponding to desulfurized products (DDS and HYD routes). A_{HYD} means the activity for the HDS hydrogenation route. A_{DDS} stands for the total activity for the HDS direct desulfurization pathway from 4,6-DMDBT and from isomerization and dismutation reactions. $A_{direct\ DDS}$ refer to the amount of products resulting from the HDS direct desulfurization. $A_{DDS\ Acid}$ concerns the amount of HDS desulfurized products resulting from the isomerization and the dismutation of 4,6-DMDBT.

The contact time, defined as the ratio between the volume of the catalyst and the gas flow of the reactant, was adapted in order to obtain a conversion of reactant of around 25% for all the catalysts. Owing to the high boiling point of the reactant and products, on-line analysis of the

reaction products was not convenient. Consequently, the reactor effluents were condensed and liquid samples were periodically collected to be analyzed by gas chromatography. Gaseous products were not found except for methane which was produced by dimethyl disulfide decomposition. Analyses were carried out with an Agilent 7820A equipped with a 30 m BP1 capillary column (inside diameter: 0.32 mm; film thickness : 5 μm) with a temperature program from 50 to 70 °C (4°C/min) then from 70 to 250°C (15 °C/min).

2.3. Characterization

Bare and impregnated supports have been characterized by SAXS nitrogen adsorption desorption analysis, pyridine adsorption desorption followed by IR, TEM and XPS.

Small angle X-Ray scattering (SAXS) measurements were carried out on a "SAXSess mc²" instrument (Anton Paar), using line-collimation system. This instrument is attached to a ID 3003 laboratory X-Ray generator (General Electric) equipped with a sealed X-Ray tube (PANalytical, $\lambda_{Cu,\ K\alpha} = 0.1542$ nm) operating at 40 kV and 50 mA. Each sample was introduced between two sheets of Kapton® then placed inside an evacuated sample chamber and exposed to X-Ray beam. Scattering of X-Ray beam was recorded on a CCD detector (Princeton Instruments, 2084 x 2084 pixels array with 24 x 24 μm² pixel size, sample-detector distance = 309 mm). Using SAXSQuant software (Anton Paar), the two-dimensional image was integrated into one-dimensional scattering intensities I(q) as a function of the magnitude of the scattering vector $q = (4\pi/\lambda) \sin(\theta)$, where 2θ is the total scattering angle. Thanks to a translucent beamstop allowing the measurement of an attenuated primary beam at $q = 0$, all measured intensities can be calibrated by normalizing the attenuated primary intensity. All data were then corrected for the background scattering from the cell and for slit-smearing effects by a desmearing procedure from SAXSQuant software, using Lake method.

Powder X-ray diffraction patterns of mesostructured TiO_2 supports were recorded at wide angles using a Panalytical X'Pert PRO diffractometer equipped with a Cu X-ray tube ($\lambda_{Cu\ (K\alpha)}$ = 0.15418 nm) operating at 45 kV and 40 mA and an X'Celerator detector. The powder patterns were collected at 25°C in the range 3<2θ<70, step= 0.017°2θ, time/step=220s.

The porosity and the specific surface area have been evaluated by nitrogen adsorption desorption at -196 °C using Micromeritics TRISTAR 3000 equipment. Isotherms were determined over a wide relative pressure range from 0.01 to 0.995. The pore diameter and the pore size distribution were obtained by applying the BJH (Barret, Joyner, Halenda) method [26] to the adsorption branch of the isotherm. Prior to analysis, 100 mg of solid is degassed at 350 °C during one night.

Raman Scattering Spectra were collected on a Jobin-Yvon T64000 spectrometer equipped with an optical microscope in confocal mode. The excitation beam (514.5 nm) was focused using a long-frontal x50 objective (numerical aperture 0.5) on an area of about 3 μm^2. The laser power on the sample was approximately 10 mW. The spectral resolution was 3 cm^{-1}, with a wavenumber precision better than 1 cm^{-1}.

The measurement of the acidity (Lewis and Brønsted) by adsorption of pyridine followed by FTIR spectroscopy was carried out with a ThermoNicolet NEXUS 5700 spectrometer at a resolution of 2 cm^{-1} and collected 128 scans per spectrum. Catalyst samples were pressed into thin pellets (10-60 mg) with diameter of 16 mm under a pressure of 1-2 $t.cm^{-2}$ and activated *in situ* during one night under nitrogen at 380°C. After cooling down the samples until room temperature, a background spectrum was collected after removal of the excess of pyridine with a vacuum pump. Lewis and Brønsted acid sites were quantified from the area of the band at 1445-1450 cm^{-1} for the Lewis acidity and at 1540 cm^{-1} for the Brønsted acidity [27,28]. All spectra were normalized to sample mass (20 mg).

A JEOL JEM2100F transmission electron microscope (TEM) was used to characterize the morphology of MoS_2 phase.

XPS spectra were collected on a Kratos Axis Ultra (Kratos Analytical, U.K.) spectrometer with a hemispherical energy analyzer and using a monochromatic Al Kα source (1486.6 eV). All spectra were recorded at a 90° take off angle, with the analyzed area being currently about 0.7 x 0.3 mm. Survey spectra were acquired with 1.0 eV step and 160 eV analyzer pass energy and the high-resolution regions with 0.1 eV step and 20 eV pass energy (instrumental resolution better than 0.5 eV). The, Co 2p, Mo 3p, Mo 3d, S 2s and S 2p binding energies were referenced to the C1s line situated at 284.6 eV, i.e. the value generally accepted for adventitious carbon surface contamination. The XPS data, reported in Table 3, of the sulfidation rate of molybdenum (TSMo), the global sulfidation degree (TSG), promotion rate (PR) and the promoter [$(Co/Mo)_{slabs}$] are calculated as follows :

$$TSMo = \frac{[MoS_2]}{[Mo]_{Total}}$$

$$TSG = \frac{[S]_{Total}}{\frac{8*[Co]_{Total}}{9} + 2*[Mo]_{Total}}$$

$$PR = \frac{[CoMoS]}{[Co]_{Total}} \text{ x } 100$$

$$\left(\frac{Co}{Mo}\right)_{Slabs} = \frac{[CoMoS]}{MoS_2}$$

3. Results and discussion:

3.1. Properties of the impregnated CoMo/TiO_2 catalysts

After impregnation of CoMo, except for P25, due to the incorporation of Mo and Co components at the surface and inside the mesopores the values of the specific surface area and of the mesopores volumes decreased by about 33-54% and 25-53%, respectively (Table 1). It

should be noted that after impregnation regardless the surfactant used, the mesostructured TiO_2 kept a high specific area of 200 m²/g after being calcined at 380°C. The second important fact is that the CoMo supported on mesostructured TiO_2 has higher specific surface area than the one supported on P25 (commercial TiO_2) and the reference catalyst CoMo supported on Al_2O_3.

However, looking at the effect of the calcination temperature, we noted a decrease of both the specific surface and the pore volume with the increase of the calcination temperature for the bare and the impregnated supports. Moreover, the mesostructure collapsed after 550°C. Indeed, after heating at 650°C no reflection was detected any longer on the SAXS pattern (Figure 1). X-ray peaks characteristic of anatase are observed on the mesostructured TiO_2 thermally treated at 380, 450 and 550°C (Figure 2). Their intensity increase when the temperature of the thermal treatment increases, confirming a higher crystallization degree. A halo due to amorphous phase in the 2θ range 25-32° is clearly observed after thermal treatment at 380°C and is barely visible after thermal treatment at 550°C. Meantime, in Raman the shift from 147 to 143 cm^{-1} of the Eg mode in the Raman spectra of mesostructured TiO_2 (Figure 3) indicated that the crystallization of the walls was enhanced when the temperature was raised. Indeed, it has been reported that the position of this vibration is dependent of the TiO_2 crystallite size [29-31]. The Eg mode appears at 143 cm^{-1} in bulk anatase and shifts to higher wavenumbers in nanocrystalline materials. So the anatase particles grew when the temperature increased from 380 to 650°C. After treatment at 650°C the appearance of the vibration at 448 cm^{-1} (Eg), revealed the presence of rutile. The other vibrations at 143 (Eg), 196 (Eg), 398 (B1g), 520 (A1g+B1g) and 642 cm^{-1} (Eg) were due to anatase. Wide-angle XRD and Raman data indicate that starting with the amorphous phase and the anatase one, the TiO_2 was transforming into anatase and rutile with the increase of the

temperature. The specific surface area dropped to 12 m^2 g^{-1} after calcination at 650°C, strengthened the growth of the anatase particles and led to a collapse of the mesostructure.

This phenomena can also explain the results of IR-pyr (**Table 2**), used to characterize the acidity properties of the titania materials. Looking at the mesoporous titania prepared according to the sol-gel method, quantification of the acidity (**Table 2**) reveals that before and after impregnation of Mo and Co Brønsted acid sites were present. The latter can be related to the semi crystalline features of the walls. Some hydroxyls groups, responsible for the Brønsted acidity, were present on the surface of the amorphous phase. Increasing the temperature treatment, the amount of Brønsted sites decreases because of the crystallization of the walls and after treatment at 650°C, no Brønsted is detected, reflecting the complete crystallization of the titania framework into anatase and rutile phase. This evolution is in accordance with literature. Indeed, Afanasiev et al. have shown only strong Lewis acid sites on anatase and rutile surfaces [32]. Alumina and P25 (75% of anatase and 25% of rutile), have only Lewis sites at their surface. The results reported below clearly show that the Brønsted acidity observed for the mesostructured titania is attributed to the presence of the amorphous phase.

It is also worth noting that for any materials the Lewis acidity is superior to the Brønsted acidity. It should finally be noted that the commercial Al_2O_3 and P25 were impregnated under the same conditions as the mesostructured titania ones.

3.2. Characterization of the sulfide phase

The parameters closely associated to the formation of the active phase such as the S/Mo, Co/Mo atomic ratios, the promotion by cobalt (PR), S/Mo atomic ratios, the sulfidation rate of molybdenum (TSMo) and the global sulfidation rate (TSG) are given in Table 3 from XPS analysis. From this table, we can conclude that whatever the support, MoS_2 has been formed.

In addition, taking into account the error on the calculation, about 20%, we can note that for the mesostructured TiO_2, whatever the temperature, the sulfidation rate of molybdenum (TSMo), global sulfidation degree (TSG), promotion rate (PR), atomic S/Mo and Co/Mo ratios are very close. This shows that the temperature of calcination of the mesostructured did not impact the formation of MoS2 phase and its promotion by the cobalt. For example, the global sufidation degree and the S/Mo ratio vary from 62 to 61 and from 1.6 to 1.2, respectively, when the calcination temperature increased from 450 to 650°C. The typical slabs of MoS_2 crystallites are observed by transmission electronic microscopy (Figure 4). From this figure, it appears that the temperature treatment affected neither the morphology nor the stacking of the slabs, which are constituted by 1 or 2 layers. By contrast the length of the slabs increased with the temperature (Figure 5A) and the slabs' length distribution became broader (Figure 5B). This variation occurred in parallel to the decrease of the Lewis and Brønsted acidities of the impregnated supports.

The characterizations indicate an effect of the thermal treatment of the mesostructured TiO_2 support on the specific surface area as well as on the acidic properties and on the slabs' length.

3.3. HDS of 4,6-DMDBT

All the catalysts were evaluated for the hydrodesulfurization (HDS) of 4,6-dimethyldibenzothiophene (4,6-DMDBT). It should be noted that whatever the catalysts, no deactivation was observed. The catalytic activities were calculated per gram of catalyst, per m^2 and per Mo atom, respectively reported in Table 4, 5, and 6 in order to have the global activities and to show the contribution of the specific surface area and to determine the modification of the activity per molybdenum atom. The catalytic performances of the different materials are compared in terms of total activity (A_T), hydrodesulfurization activity

(A_{HDS}), acid activity (A_{Acid}), activities of the different routes (A_{DDS}, A_{HYD}, $A_{direct\ DDS}$, $A_{Acid\ DDS}$), selectivity of transformation routes and of HYD/DDS ratio. As reported in Table 4 (specific activity), catalysts with mesostructured TiO_2 thermally treated at 380 and 450°C as supports had a higher total activity (A_T) and HDS activity (A_{HDS}) than with P25 or Al_2O_3 as supports. Differences were observed for the activities in HDS (A_{HDS}) and involving the Brønsted acidity ($A_{acid.}$). As reported previously [18,19], mesostructured TiO_2 induced the presence of Brønsted acidity which decreased with the temperature of the treatment of TiO_2 mainly at 550°C and 650°C. In the same way a high decrease of the total activity (A_T), HDS activity (A_{HDS}) and of Acid activity ($A_{Acid.}$) from 550°C to become very low at 650°C was observed. This corresponds also to a more important crystallization of the walls of the support into anatase, to a high decrease of the specific surface area and also to a lower amount of molybdenum (its deposition depended on the specific area: 3atom per nm^2). In order to distinguish the impact of these different parameters, we looked at the same activity per m² (Table 5) and at the same amount of molybdenum atom (Table 6). A decrease in total activity can still be seen, but this decrease is only due to a drop of the A_{Acid}, A_{HDS} is constant between 380°C and 550°C (Table 5). The correlation with the physico-chemicals properties (**Table 1**) explains these results, the diminution of total activity per gram is due to the loss of the specific surface area and the **Table 2** shows the importance of the Brønsted acidity because the loss of the latter leads to a decrease of total activity per m² for a thermal treatment from 380°C to 650°C. These observations are confirmed by the Table 6 which allows us to understand that there is no significant change in the Mo atom environment and no change of the active sites for a thermal treatment of the mesostructured titania from 380°C to 650°C. These results were also confirmed taking into account to only the amount of mixed CoMoS phase (not reported here).

Finally, the significant conclusion of this study is that using TiO_2 support prepared by the surfactant templating method, whatever the heating temperature the DDS pathway remains the main route for 4,6-DMDBT desulfurization. On mesostructured TiO_2, DDS (Direct + Acid) (mainly DDS Direct) became the major pathway in contrast to alumina where HYD is the main route. This change mainly comes from the modification of the direct DDS which contributes to around 50 % of the overall DDS for CoMoS/TiO_2 whatever the temperature of the treatment excepted at 380°C (43%). The other part is due to the presence Brønsted acidity which represents less than 15% of the DDS excepted at 380°C (22%). The consequence is a decrease of a HYD/DDS ratio from 3 in the presence of Al_2O_3 as support to 0.54 for TiO_2 (treated at 380°C) as support. Only a small HYD/DDS ratio difference was noticed for the different treatment temperatures (from 0.54 to 0.73). The HYD/DDS ratio with P25 as support is intermediate between TiO_2 and Al_2O_3 as supports. The change of selectivity (HYD/DDS) observed with CoMo/TiO_2 is unique and due to the intrinsic properties of the mesoporous TiO_2, as the temperature of the thermal treatment does not change the selectivity. A calcination temperature of 380°C seems to be the best temperature of the treatment of TiO_2 leading to the higher contribution of the Brønsted acidity in the HDS activity.

4. Conclusion

Mesostructured titania used as a support of hydrotreating catalysts, in particular 4,6-dimethyldibenzothiophene, is of great interest. Indeed, it increases the global activity and involves a change of selectivity for HDS of 4,6-DMDBT toward the direct desulfurization route, compared to the reference catalyst CoMo supported over Al_2O_3. This change of selectivity is due to the increase of the direct DDS route in one hand and to DDS route resulting of isomerization and dismutation reactions involving Brønsted acidity, in the other hand. The temperature of the thermal treatment of the mesostructured titania support is a key

parameter in the catalytic activity but not on the selectivity of the transformation pathways. A thermal treatment at 380°C leads to the formation of semi-crystalline mesostructured TiO_2 with high specific surface area. A thermal treatment at higher temperature (650°C) leads to a decrease of the specific surface area and to an almost complete crystallization of the walls into mainly anatase and rutile. This result shows that the mesostructured titania has unique properties that allow the direct desulfurization to be favoured. Mesoporous titania offers new perspectives to develop an eco-efficient HDS process reducing the consumption of hydrogen during hydrodesulfurization process leading to cleaner fuel, maintaining high desulfurization activity.

Acknowledgments

We would like to thank the platform "Spectroscopies et Microscopies des Interfaces", Martine Mallet and Aurélien Renard (LCPME) for XPS analyses. The platform "X-ray diffusion" of IS2M is also acknowledged.

References

[1] « https://www.transportpolicy.net/?s=sulfur (accessed on 23/04/2019)».

[2] X. Ma, K. Sakanishi, I. Mochida, Ind. Eng. Chem. Res. 33 (1994) 218-222.

[3] S.S. Shih, S. Mizrahi, L.A. Green, M.S. Sarli, Ind. Eng. Chem. Res. 31 (1992) 1232-1235.

[4] T. Kabe, A. Ishihara, H. Tajima, Ind. Eng. Chem. Res. 31 (1992) 1577-1580.

[5] D.D. Whitehurst, T. Isoda, I. Mochida, Adv. Catal. 42 (1998) 345-471.

[6] M.V. Landau, Catal. Today 36 (1997) 393-429.

[7] X. Ma, K. Sakanishi, I. Mochida, Ind. Eng. Chem. Res. 35 (1996) 2487-2494.

[8] F. Bataille, J.L. Lemberton, P. Michaud, G. Pérot, M. Vrinat, M. Lemaire, E. Schulz, M. Breysse, S. Kasztelan, J. Catal. 191 (2000) 409-422.

[9] G. Pérot, Catal. Today 86 (2003) 111-128.

[9] H. Farag, I. Mochida, K. Sakanishi, Appl. Catal. A Gen. 194-195 (2000) 147-157.

[10] W.Zhou, Y. Zhou, Q. Wei, L. DU, S. Ding, S. Jiang, Y. Zhang, Q. Zhang, Chem. Eur. J. 23 (2017) 9369-9382.

[11] A.Stanislaus, A.Marafi, M.S. Rana, Catal. Today 153 (2010) 1-68.

[12] V. Sundaramurthy, I. Eswaramoorthi, A.K. Dalai, J. Adjaye, Microporous and Mesoporous Mater.111 (2008) 560-568.

[13] T. Klimova, L. Peña, L. Lizama, C. Salcedo, O. Y. Gutiérrez, Ind. Eng. Chem. Res. 48 (2009) 1126–1133.

[14] J.C. Duchet, M.J. Tilliette, D. Cornet, L. Vivier, G. Perot, L. Bekakra, C. Moreau, G. Szabo, Catal. Today 10 (1991) 579-592.

[15] G. M. Kumaran, S. Garg, K. Soni, V. V. D. N. Prasad, L. D. Sharma, G. Murali Dhar, Energy & Fuels, 20 (2006) 1784-1790.

[16] M. Breysse, P. Afanasiev, C. Geantet, M. Vrinat, Catal. Today 86 (2003) 5-16.

[17] N. Prabhu, A.K. Dalai, J. Adjaye, Applied Catalysis A: General 401 (2011) 1- 11.

[18] I. Naboulsi, C. F. Linares Aponte, B. Lebeau, S. Brunet, L. Michelin, M. Bonne J. L. Blin, Chem. Commun. 53 (2017) 2717-2720.

[19] I. Naboulsi, B. Lebeau, C. F. Linares Aponte, S. Brunet, M. Mallet, L. Michelin, M. Bonne, C. Carteret, J.L. Blin, Applied Catalysis A, General 563 (2018) 91–97

[20] J. C. Morales-Ortuno, R. A. Ortega-Domingueza, P. Hernandez-Hipolito, X. Bokhimi, T. E. Klimova, Catal. Today 271 (2016) 127-139.

[21] J. Ramirez, G. Macias, L. Cedeno, A. Guitierrez-Alejandre, R. Cuevas, P. Castillo, Catal. Today 98 (2004) 19-30.

[22] H. Wang, X. Cheng Catal. Surv. Asia 19 (2015) 78-87.

[23] K. Zimny, J. Ghanbaja, C. Carteret, M.J. Stébé New J. Chem. 34 (2010) 2113-2117.

[24] K. Zimny, C. Carteret, M.J. Stébé, J.L. Blin J. Phys. Chem. C 116 (2012) 6585-6594.

[25] Naboulsi, B. Lebeau, L. Michelin, C. Carteret, L. Vidal, M. Bonne, M.J. J.L. Blin, ACS Appl. Mater. Interfaces 9 (2016) 3113-3122.

[26] E.P. Barrett, L.G. Joyner, P.P. Halenda, J. Am. Chem. Soc. 73 (1951) 373-380.

[27] J.C Lavalley, R. Anquetil, J. Czyziewska, M. Ziolek, J. Chem. Soc. Trans., 92 (1996) 1263-1266.

[28] M. V. Zakharova, F. Kleitz, F.G. Fontaine, Dalton Trans., 46 (2017) 3864-3876.

[29] S. Kelly, F.H. Pollak, M. Tomkiewicz, J. Phys. Chem. B 101 (1997) 2730-2734.

[30] W.F. Zhang, Y.L. He, M.S. Zhang, Z. Yin, Q. Chen, J. Phys. D: Appl. Phys. 33 (2000) 912-916.

[31] A. Pottier, S. Cassaignon, C. Chanéac, F. Villain, E. Tronc, J.P. Jolivet, J. Mater. Chem. 13 (2003) 877-882.

[32] H. Li, M. Vrinat, G. Berhault, D. Li, H. Nie, P. Afanasiev, Mater. Res. Bull. 48 (2013) 3374-3382.

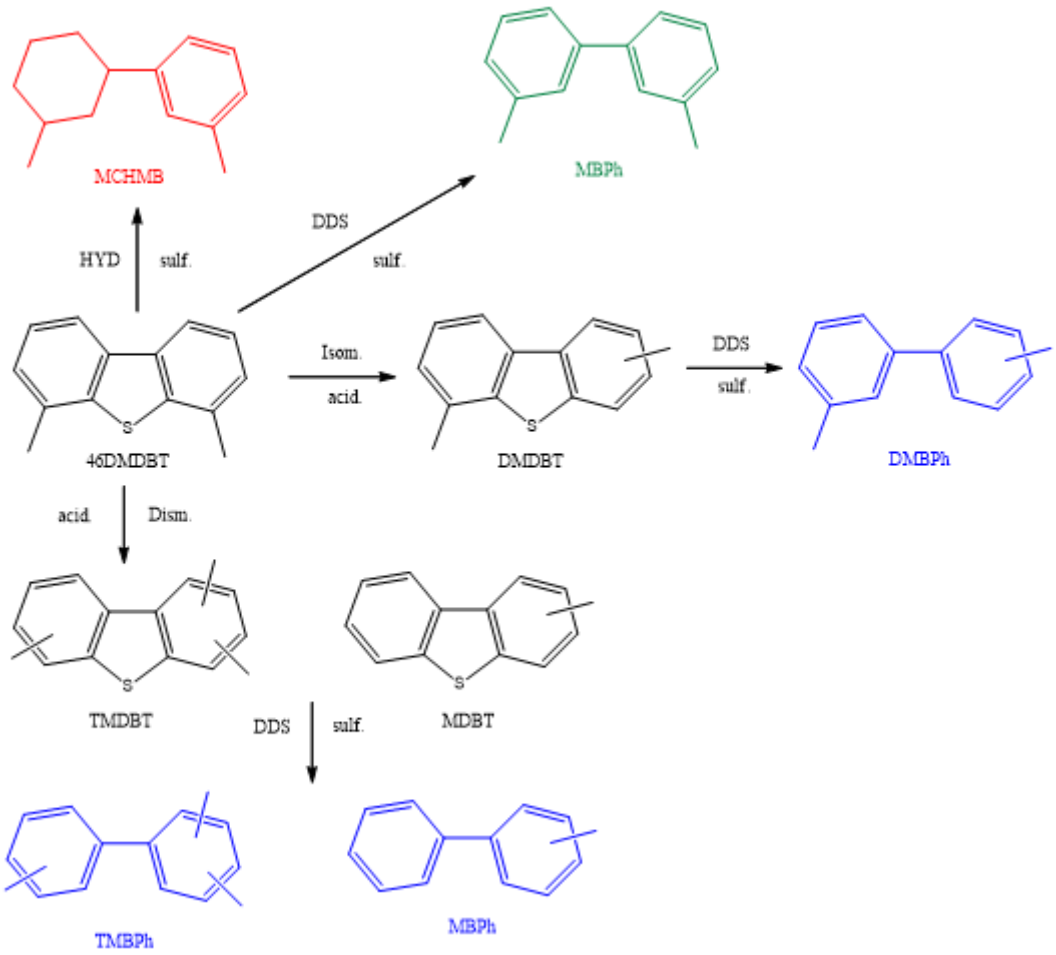

Scheme 1 : Transformation of 4,6-DMDBT over CoMoS/TiO_2. (HYD: Hydrogenation route, DDS: Direct desulfurization route, sulf: sulfide phase, acid: acid properties, Dism : Dismutation, Isom: Isomerization. 4,6-DMDBT: 4,6 dimethyldibenzothiophene, MCHMB, methylcyclohexylmethylbenzene, MBPh: methylbiphenyl, DMDBT: dimethyldibenzothiophene, DMBPh: dimethylbiphenyl, TMDBT: trimethylbiphenyl, MBPh: methylbiphenyl.

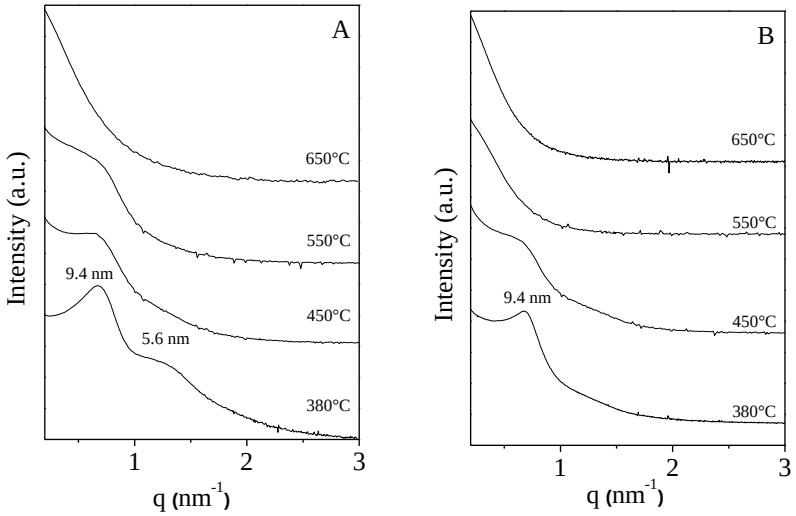

Figure 1: Evolution of the SAXS patterns of the mesostructured TiO_2 supports as a function of the calcination temperature before (A) and after (B) impregnation by Co and Mo.

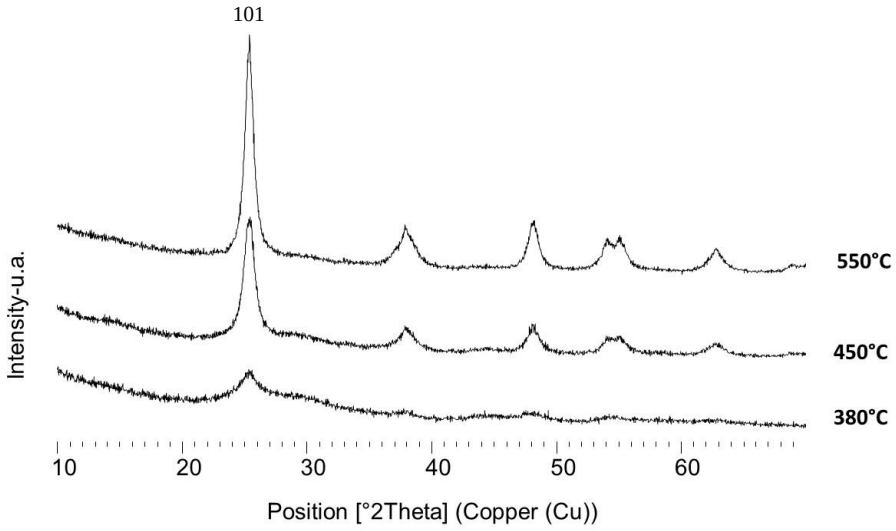

Figure 2: XRD pattern of TiO_2 at different temperature of thermal treatment

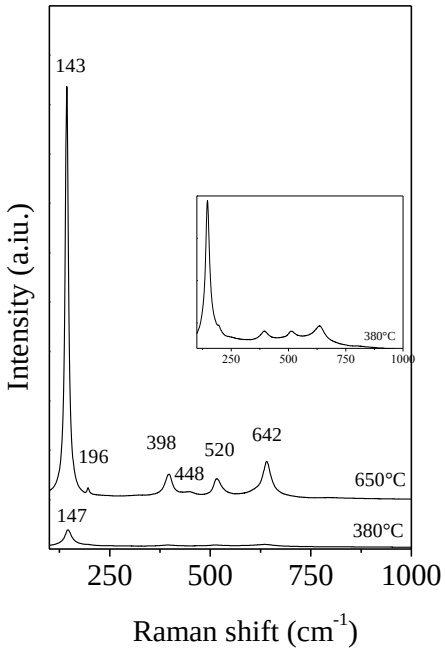

Figure 3: Raman spectra of the mesostructured TiO_2 support after calcination at 380 and 650°C.

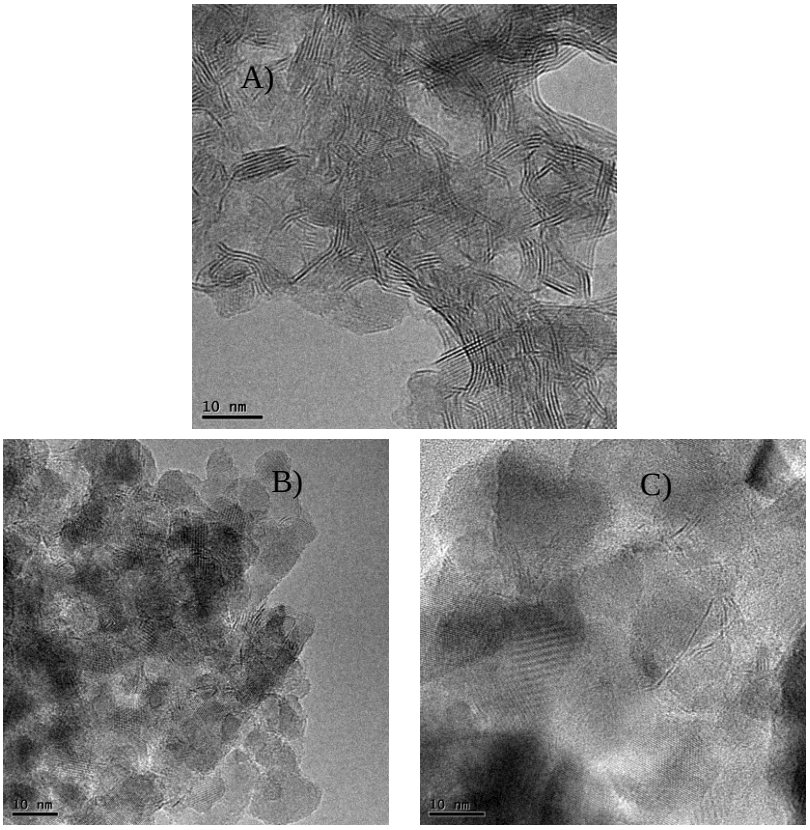

Figure 4: TEM images of the $CoMoS/TiO_2$ catalysts depending on the temperature of treatment of the TiO_2 support A) 450°C, B) 550°C, C) 650°C

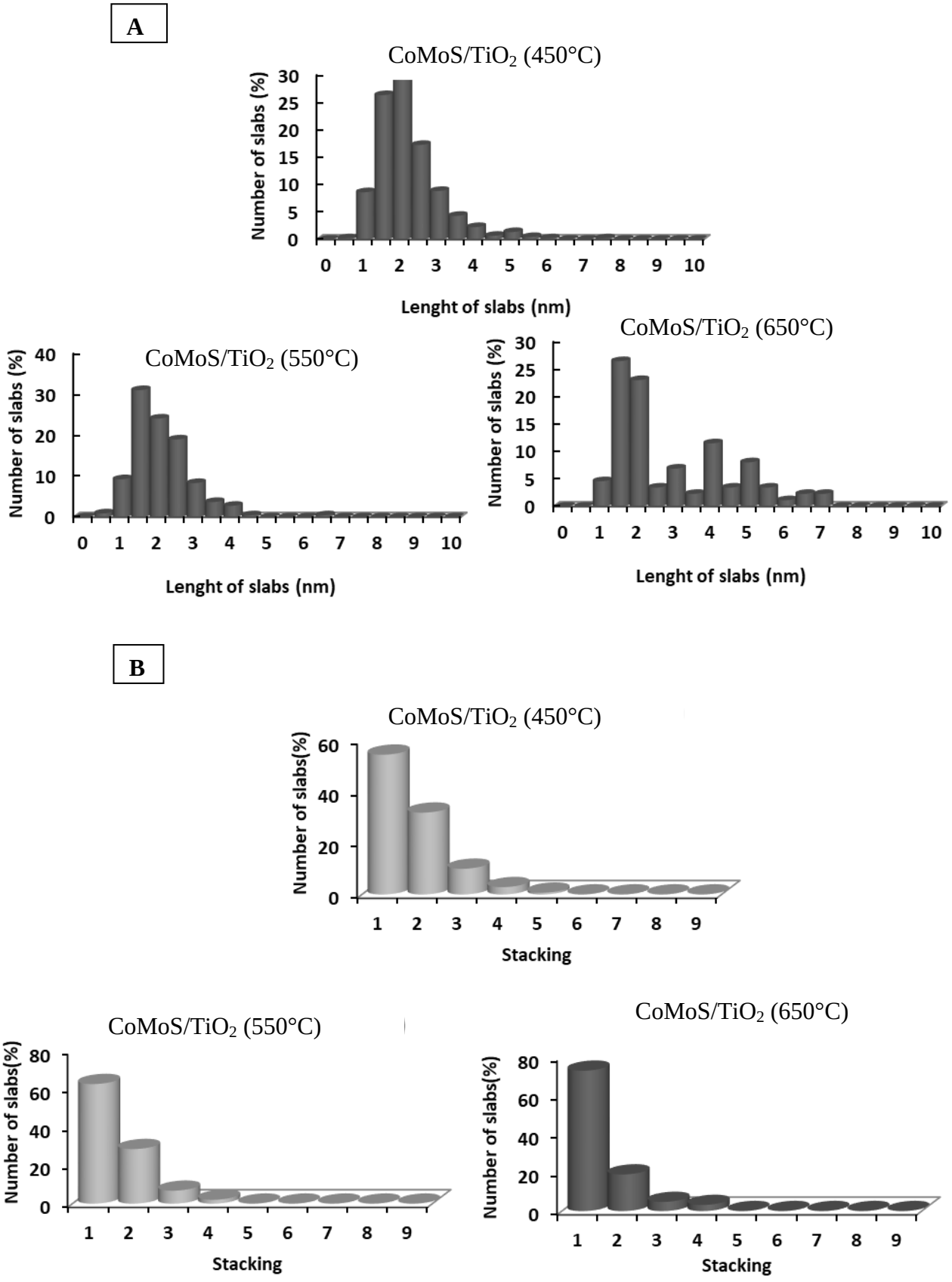

Figure 5: Histograms of the slab distribution as a function of length (A) and of their stacking (B)

Table 1 : Specific surface area (S_{BET}), pore diameter (Ø) and mesopore pore volume (V_P) of the supports before and after impregnation.

Support	T_{calci} (°C)	Before impregnation			After impregnation			MoO_3 (%)	CoO (%)
		S_{BET} ($m^2.g^{-1}$)	Ø* (nm)	Vp* ($cm^3.g^{-1}$)	S_{BET} ($m^2.g^{-1}$)	Ø* (nm)	Vp* ($cm^3.g^{-1}$)	0	0
P25		37	-	-	37	-	-	2.6	0.7
TiO_2	380	300	6.5	0.40	200	6.6	0.33	21.5	4.0
	450	180	6.3	0.30	130	5.6	0.27	12.9	2.6
	550	130	5.5	0.23	106	4.8	0.15	9.3	2.1
	650	12	-	0.03	6	-	0.02	0.9	0.1

*Values determined from the BJH method applied to the adsorption branch of the isotherm.

Table 2 : Lewis (L) and Brønsted (B) acidity measurement by FTIR pyridine of TiO_2 after wet impregnation.

CoMo/ Support	$T_{treatment}$ (°C)	n_{pyr} (µmol.g^{-1})		n_{pyr} (µmol.m^{-2})		B/L
		L	B	L	B	
Al_2O_3	-	140	0	1.1	0	0
P25	380	140	3	3.8	0.08	0.02
TiO_2	380	344	85	1.6	0.41	0.25
	450	325	39	2.5	0.30	0.12
	550	276	15	2.6	0.14	0.05
	650	124	0	10.3	0	0

Table 3: Sulfidation rate of molybdenum (TSMo), global sulfidation degree (TSG), promotion rate (PR), atomic S/Mo and Co/Mo ratios and promoter ratio [$(Co/Mo)_{slabs}$]. Data are obtained from XPS analysis.

Support	T°C	TSMo (%)	TSG (%)	PR[a] (%)	S/Mo	Co/Mo	$(Co/Mo)^{b}_{slabs}$
TiO_2	380	53	69	36	1.8	0.3	0.19
	450	47	62	51	1.6	0.3	0.31
	550	57	84	46	1.8	0.3	0.28
	650	56	61	-	1.2	0.5	-
P25*	380	40	71	13	2.3	0.4	0.13
γ-Al_2O_3**	-	70	53	26	1.5	0.3	0.10

* used as TiO_2 reference
** used as reference for HDS reactions

a : $PR = \frac{[CoMoS]}{[Co]_{Total}} \times 100$

b : The promoter ratio is the Co/Mo ratio in the slabs [$(Co/Mo)_{slabs}$]

$$\left(\frac{Co}{Mo}\right)_{Slabs} = \frac{[CoMoS]}{MoS_2}$$

- not determined

Table 4: Transformation of 4,6-DMDBT : Effect of the calcination temperature of the mesostructured TiO_2 support, detailed of the total activity (A mmol h^{-1} g^{-1}) compared with reference catalyst (P25 and Al_2O_3). The selectivity (%) of each pathway of hydrodesulfurization is given (T = 340°C, P = 40 bars, H_2/feed = 475 NL/L)

		Activity (mmol h^{-1} g^{-1})			Selectivity (%)			
CoMo/ Support	$T_{treatment}$ (°C)	A_T	A_{HDS}	A_{Acid}	HYD	DDS Direct	DDS Acid	HYD/DDS
TiO_2	380	1.61	0.98	0.39	35	43	22	0.54
	450	1.19	0.89	0.30	38	48	14	0.62
	550	0.65	0.52	0.13	42	52	6	0.73
	650	0.09	0.06	0.03	37	50	13	0.59
P25	380	0.24	0.20	0.04	50	50	0	1
Al_2O_3	-	0.73	0.73	0	75	25	0	3

A_T = Total activity, sum of acid activity and hydrodesulfurization activity

A_{HDS} = Total activity of hydrodesulfurization, DDS and HYD pathways

A_{Acid} = Total activity of isomerization and dismutation routes leading to no desulfurized products

Table 5: Transformation of 46DMDBT: Effect of the calcination temperature of the mesostructured TiO_2 support, detailed of the total activity (A mmol h^{-1} m^2) compared with reference catalyst (P25 and Al_2O_3) (T = 340°C, P = 40 bars, H_2/feed = 475 NL/L).

		Activity (mmol h^{-1} m^{-2}) x 10^{-3}						
CoMo/ Support	$T_{treatment}$ (°C)	A_T	A_{HDS}	A_{Acid}	A_{HYD}	A_{DDS}	$A_{DDS\ Direct}$	$A_{DDS\ Acid}$
TiO_2	380	8.1	4.9	3.2	1.7	3.2	2.1	1.1
	450	7.0	5.2	1.9	2.0	3.2	2.5	0.7
	550	6.1	4.9	1.2	2.1	2.8	2.5	0.3
	650	14	10.9	3.1	4.6	6.3	5.6	0.7
P25	380	6.4	5.4	1.0	2.7	2.7	2.7	0
Al_2O_3	380	6.0	6.0	0	4.5	1.5	1.5	0

A_T = Total activity, sum of acid activity and hydrodesulfurization activity

A_{HDS} = Total activity of hydrodesulfurization, DDS and HYD pathways

A_{Acid} = Total activity of isomerization and dismutation routes leading to no desulfurized products

A_{DDS} = Activity of direct desulfurization (A_{DDS} Direct) + activity of DDS of the acid route (A_{DDS} Acid)

A_{HYD} = Activity of desulfurization by the HYD route

Table 6: Transformation of 46DMDBT : Effect of the calcination temperature of the mesostructured TiO_2 support, detailed of the total activity (A mmol h^{-1} Mo $atom^{-1}$.) compared with reference catalyst (P25 and Al_2O_3) (T = 340°C, P = 40 bars, H_2/feed = 475 NL/L).

		Activity (mmol h^{-1} Mo $atom^{-1}$.) x 10^{-21}						
CoMo/ Support	$T_{treatment}$ (°C)	A_T	A_{HDS}	A_{Acid}	A_{HYD}	A_{DDS}	$A_{DDS\ direct}$	$A_{DDS\ Acid}$
TiO_2	380	1.5	1.1	0.4	0.4	0.7	0.5	0.2
	450	2.2	1.6	0.6	0.6	1.0	0.9	0.1
	550	1.7	1.3	0.3	0.6	0.8	0.7	0.1
	650	2.5	1.7	0.8	0.6	1.1	0.8	0.2
P25	380	2.1	1.8	0.3	0.9	0.9	0.9	0.0
Al_2O_3	-	2.0	2.0	0.0	1.5	0.5	0.5	0.0

A_T = Total activity, sum of acid activity and hydrodesulfurization activity

A_{HDS} = Total activity of hydrodesulfurization, DDS and HYD pathways

A_{Acid} = Total activity of isomerization and dismutation routes leading to no desulfurized products

A_{DDS} = Activity of direct desulfurization (A_{DDS} Direct) + activity of DDS of the acid route (A_{DDS} Acid)

A_{HYD} : Activity of desulfurization by the HYD route